THE AMERICAN MINERALOGIST, VOL. 56, JANUARY-FEBRUARY, 1971

STABILITY AND PHYSICAL PROPERTIES OF SYNTHETIC LITHIUM-IRON MICAS

MILAN RIEDER[1], *Department of Earth and Planetary Sciences, Johns Hopkins University, Baltimore, Md. 21218.*

ABSTRACT

Stability of micas on the siderophyllite-polylithionite join was studied at 2 kbar in atmosphere controlled by the calcite-fluorite-graphite buffer with $f(H_2)$ of the nickel-nickel oxide buffer imposed externally. These micas have an extensive stability field below 550°C. Siderophyllite reacts to kalsilite+hercynite+cation-deficient siderophyllite at ~570°C, polylithionite, to sanidine+lithium metasilicate at ~550°C. Mica sid $_{5.5}$pl$_{2.5}$ is stable above 800°C and so are cation-deficient iron-rich micas.

Buffered micas are octahedrally disordered (indicated by cell data), while natural micas are ordered. This is because f(HF) of the buffer is lower than in nature. The shape of the stability field of buffered micas is similar to that of natural micas because the most frequent natural compositions are close to most stable synthetic compositions.

Cation deficiency was found in iron-rich synthetic micas. In order to become deficient, the mica extracts silica from the system. This process depends on fugacities of volatiles and affects negligibly cell dimensions of the mica. Cation deficiency is expected to augment and expand to lithium-rich compositions in presence of quartz and if f(HF) is higher. Fluorine lowers the stability of annite, favoring siderophyllite, which agrees with observations from nature.

INTRODUCTION

The preceding papers on lithium-iron micas (Rieder *et al.*, 1970, 1971; Rieder, 1968a, 1970) dealt with chemical composition, physical properties, and crystallography of natural lithium-iron micas from greisens and hydrothermal veins in the Krušnéhory Mts. (Czechoslovakia) and Erzgebirge (German Democratic Republic). The conclusions of this study are that (*i*) the chemical variation of natural lithium-iron micas and crystallography fit best the join siderophyllite-polylithionite; (*ii*) along this series, there is an approximately 1:1 relation between atomic quantities of lithium and fluorine; (*iii*) the octahedral sheet of natural lithium-iron micas contains close to two trivalent cations[2] and an irregular number of Li and Fe^{2+} (plus some Mg and Mn^{2+}) accompanied by vacancies; (*iv*) polytypism shows no relation to chemical composition along the series except for the 120° motif in stacking; (*v*) natural micas have relatively small basal spacings and appear to be octahedrally ordered. Synthetic micas ought to reflect all these features. As the first step, idealized com-

[1] Present address: Ústav geologických věd University Karlovy (Institute of Geological Sciences, Charles University), Albertov 6, Praha 2, Czechoslovakia.

[2] Elements in micas are referred to as anions and cations for brevity; their bonding may not be purely ionic.

positions along the join $K_2Fe_4^{2+}Al_2Al_4Si_4O_{20}(OH, F)_4$ (siderophyllite)-$K_2Li_4Al_2Si_8O_{20}(F, OH)_4$ (polylithionite) were synthesized and their stabilities studied at 2 kbar in a controlled C-F-H-O atmosphere. Synthesis experiments were performed also on related and cation-deficient compositions. Cell parameters and refractive indices of synthetic micas were compared to those of natural micas.

Fluorine in Micas

The variation of fluorine content in natural lithium-iron micas (little or no fluorine in siderophyllite, close to F_4 in polylithionite), demands that it be one of the variables in their synthetic counterparts. Besides, it had been known that fluorine affects seriously the stability of micas; at one atmosphere, fluoro-phlogopite breaks down at 1345°C (van Valkenburg and Pike, 1952), hydroxy-phlogopite, at 770°C (Yoder and Eugster, 1954). Munoz (1966) easily synthesized fluoro-polylithionite, but failed to synthesize hydroxy-polylithionite. Siderophyllite that could not be synthesized in its hydroxy-form (Rutherford, 1968) could be grown easily in 100 percent yields from a mix with F:OH = 1:1 (this paper). The same pattern holds for lithium-iron micas; with ample fluorine in charge, any composition along the siderophyllite-polylithionite join could be synthesized; with decreasing fluorine, the synthesis was increasingly difficult or impossible.

To study stabilities of micas at different fluorine concentrations involves a tedious procedure of analyzing mica and vapor (Noda and Yamanishi, 1964; Noda and Ushio, 1964). Besides, the stability of iron-containing micas is a function of oxygen fugacity. It is thus desirable to control both fluorine and oxygen. Munoz (1966) devised a scheme of imposing independent hydrogen and oxygen fugacities on the charge in an F-H-O atmosphere, which has not been tested yet. Control of oxygen and fluorine in the atmosphere by a solid fluorine and a solid hydrogen buffer proved feasible and yielded data used in Rieder (1968a, b). Munoz (1969) rediscovered this technique, and Munoz and Eugster (1969) gave a detailed account of fluorine buffers and presented the calculated fugacities for individual buffers.

In this study, the assemblage nickel-nickel oxide (NNO) was used as hydrogen buffer, the assemblage calcite-fluorite-graphite (CFG) as fluorine buffer. Inasmuch as contamination of the charge with Ca from the fluorine buffer could not be precluded, the stabilities determined should not be interpreted in terms of $f(H_2)$ and $f(HF)$ alone, but rather as stabilities of assemblages i.e.w. calcite, fluorite, and graphite, with $f(H_2)$ imposed externally.

Experimental

Experiments were done in standard cold-seal bombs (Tuttle, 1949), p(total) was measured with a Heise bourdon gauge. The temperature was controlled by Honeywell Pyr-O-Vane controllers equipped with mercury relays and measured with chromel-alumel thermocouples on a Leeds and Northrup potentiometer standardized with a 0°C bath. This system was periodically calibrated against melting points of NaCl and Zn. The temperature in the charge lies within $\pm 5°$ C from the temperature measured in a well in the bomb. The reactions studied proved slow enough so that no special quenching technique was needed.

The charge was placed in a crimped Ag tube (0.071″O.D.) that together with 20 to 25 mg distilled water and CFG buffer occupied the inside of a sealed Ag-Pd tube (0.118″ O.D.). The NNO buffer, 25 to 30 mg distilled water, and the sealed Ag-Pd tube were placed inside a sealed Ag tube (0.173″O.D.) (Fig. 1). Synthesis runs were performed in sealed Ag-Pd or Ag tubes that contained reduced oxide mix and water. In some synthesis runs, high hydrogen pressure was needed; such runs were performed in sealed Ag-Pd tubes with benzoic acid as the source of hydrogen.

The micas were synthesized from oxide mixes. Mixes containing iron were reduced in a stream of hydrogen (~420°C, 1½ hours). The reduction was performed on a stoichiometric mixture of silica, alumina, and Fe_2O_3, with which were later combined the other chemicals.

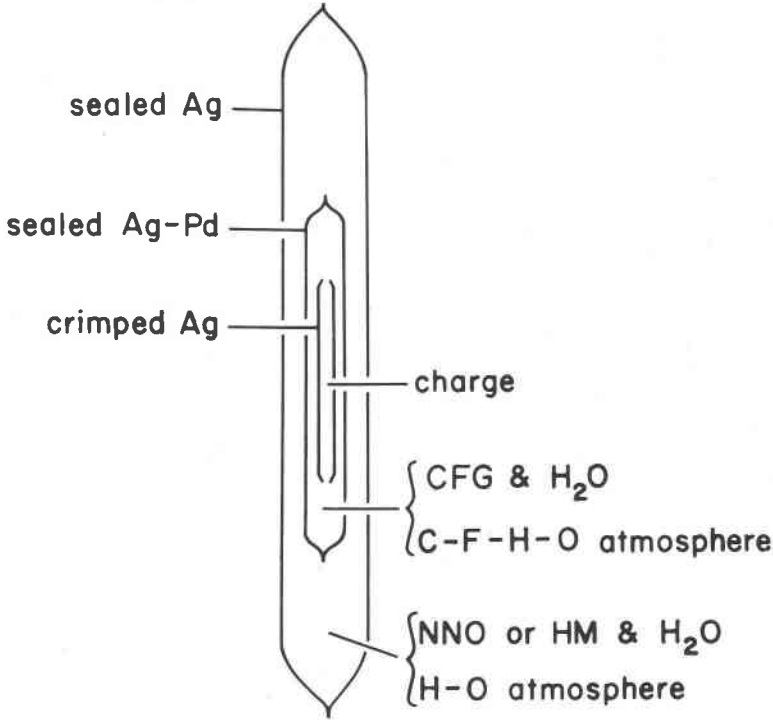

Fig. 1. A cutaway sketch of arrangement of capsules used in experiments with solid fluorine buffer.

For mixes and buffers the following chemicals were used: K_2SiF_6 (K & K Laboratories); $KHCO_3$ (Fisher Certified Reagent, lot #791147); Fe_2O_3 (Fisher Certified Reagent, lot #780323, fired in oxygen at ~700°C for two hours); γ-Al_2O_3 (prepared by firing $AlCl_3 \cdot 6H_2O$ ('Baker Analyzed' Reagent, lot #26373) in air at ~1000°C for 30 minutes); SiO_2 (prepared by firing of silicic acid ('Baker Analyzed' Reagent, lot #26001) in air at ~1300°C for 10 hours); Li_2CO_3 ('Baker Analyzed' Reagent, lot #24361); Ni (Fisher Laboratory Chemical, lot #783281); NiO (Fisher Certified Reagent, lot #792341); Fe_3O_4 (Fisher Laboratory Chemical, lot #710453); $CaCO_3$ (Fisher Certified Reagent, lot #791410); C (specpure graphite rod by Union Carbide); CaF_2 (optically clear natural fluorite); C_6H_4COOH (Fisher Certified Reagent, lot #743732). Care was taken that alumina contain no corundum and that silica be in α-cristobalite form.

Products of experiments were identified by X-ray powder and standard optical techniques. Unit-cell dimensions were calculated from diffractometer patterns (scan $\frac{1}{4}°\text{min}^{-1}$) recorded with silicon internal standard (its a taken as 5.43062 Å at 21°C); the lattice-constant refinement program was used (Burnham, 1962). Theoretical spacings were calculated from cell data using the program of Jeitschko and Parthé[1]. Single-crystal cell data were determined with a precession camera calibrated with analytical-grade NaCl and natural quartz from Lake Toxaway, N. Y.; films were corrected for shrinkage or expansion. Refractive indices were measured by immersion technique at 22°C in sodium light on an Abbé refractometer.

Description of Synthetic Phases

Annite was synthesized from OH and $F_2(OH)_2$ mixes. Both products are similar in appearance. Pleochroism is $\beta, \gamma > \alpha$. The color is dark greenish gray along β, γ (somewhat brighter in fluorine-bearing annite) and yel low to light brown along α. Refractive indices β, γ of the OH-annite lie between 1.692 and 1.703, which agrees with data of Wones (1963). Only index of refraction n could be measured for the fluorine-buffered annite, and it is 1.654 (10). Annite equilibrated with the CFG/NNO buffer has similar colors to OH-annite. X-ray patterns of all annites are analogous to that given by Eugster and Wones (1962). Cell data of annites are discussed below (Table 1).

Micas on the siderophyllite-polylithionite join. None of these micas could be grown in good yields from OH mixes. The starting micas were grown from $F_2(OH)_2$ mixes except for polylithionite, which had to be grown from an F_4 mix. Fluorine content in the mix affects both color and grain size of the resulting mica: OH-zinnwaldite (poor yields) is very fine grained (~0.002 mm) and its color is bluish green; $F_2(OH)_2$-zinnwaldite mix yields 100 percent mica of green to light olive (β, γ) and light yellow (α) color whose grain size is considerably bigger; mica grown from the F_4 mix forms six-sided plates up to ~0.2 mm in size and its color is light

[1] A Fortran IV program for the intensity calculation of powder patterns, University of Pennsylvania, Philadelphia, Pa., 1966.

TABLE 1. UNIT-CELL DIMENSIONS OF ANNITE BUFFERED WITH THE CFG/NNO BUFFER AT 2 kbar AND $T \doteq 560°C$

Starting annite[a]	T, °C (measured)	Buffering by CFG/NNO time, hours	a, Å	b, Å	$d(001)$, Å	β, °
OH	(647¾–650)	0	5.394 (2)	9.348 (3)	10.147 (4)	100.03 (4)
OH	565–575	375	5.391 (3)	9.344 (4)	10.143 (5)	100.05 (4)
OH	556-564	621½	5.392 (3)	9.346 (4)	10.147 (4)	100.04 (4)
$F_2(OH)_2$	(~557)	0	5.389 (3)	9.344 (3)	10.071 (4)	100.14 (4)
$F_2(OH)_2$	572½–576¾	306	5.394 (1)	9.341 (2)	10.147 (3)	100.06 (2)
$F_2(OH)_2$	560¼–563¾	360	5.384 (3)	9.332 (4)	10.135 (4)	100.03 (4)
$F_2(OH)_2$	569½–575¾	604½	5.392 (1)	9.338 (2)	10.137 (3)	100.06 (2)
$F_2(OH)_2$	552–568¾	869	5.391 (2)	9.333 (3)	10.136 (4)	100.07 (3)
$F_2(OH)_2$[b]	(555½–564½)	0	5.388 (3)	9.325 (3)	10.091 (5)	100.11 (3)
$F_2(OH)_2$[b]	561–562½	60	5.386 (3)	9.328 (5)	10.144 (4)	100.04 (4)
$F_2(OH)_2$[b]	559–561	133¾	5.383 (2)	9.336 (3)	10.138 (4)	100.02 (3)
$F_2(OH)_2$[b]	567¾–569½	200	5.382 (2)	9.330 (3)	10.137 (4)	100.03 (3)

[a] The starting annite is described in terms of the starting mix.

[b] This annite had been allowed to pre-equilibrate with the NNO buffer for at least 200 hours at 2 kbar and ~560°C.

olive brown (β, γ) to grayish yellow (α). At approximately constant fluorine content, the color of micas varies regularly with composition:

	siderophyllite	*zinnwaldite*	*polylithionite*
along β, γ:	dark olive gray to dark greenish gray	grayish green to light olive	colorless
along α:	light olive brown to yellow	light yellow to yellow	colorless

All colored micas in the series exhibit pleochroism $\beta, \gamma > \alpha$. Refractive indices β,γ of micas equilibrated with the buffer change as follows:

sid_8pl_0	sid_7pl_1	sid_6pl_2	sid_5pl_3	sid_4pl_4	sid_3pl_5
1.653–62	1.641–53	1.625–36	1.619–25	1.602–09	1.582–90

Iron-rich micas tend to form automorphic crystals and so do micas in buffered runs equilibrated at high temperatures. This is due partly to high temperature alone, partly to the increase of f(HF) imposed by the buffer at high temperature (Munoz and Eugster, 1969). Micas whose composition changed during the run are finer grained and rarely form six-sided plates. Cell dimensions of micas on the siderophyllite-polylithionite join are discussed below (Table 3).

Sanidine. In most assemblages sanidine forms irregular grains ~0.01 mm in size. In runs of fluoro-polylithionite composition sanidine grew as

TABLE 2. SELECTED EXPERIMENTS ON THE REACTION ANNITE⇌SANIDINE+MAGNETITE +VAPOR AT 2 kbar. ATMOSPHERE CONTROLLED BY CFG/NNO BUFFER

Reactants[a]	T, °C (measured)	Time, hours	Products
OH-ann	564–572	1200	ann+san+mt
$F_2(OH)_2$-ann	$577\frac{1}{4}$–$579\frac{1}{2}$	$639\frac{1}{2}$	san+mt
$F_2(OH)_2$-ann	$572\frac{1}{2}$–$576\frac{3}{4}$	306	ann
san+mt+ann	571–$577\frac{1}{4}$	$909\frac{1}{2}$	san+mt
san+mt	$558\frac{1}{2}$–566	$1172\frac{3}{4}$	san+mt+ann
san+mt	$551\frac{1}{2}$–567	$1172\frac{3}{4}$	san+mt+ann

[a] Prefixes OH- and $F_2(OH)_2$- refer to composition of the mix from which the mica was grown.

ann=annite; mt=magnetite; san=sanidine

euhedral crystals up to 1 mm in size that were bounded by forms {010} {001}, and {110} and elongated a. Precession work done on one crystal confirmed its monoclinic symmetry (diffraction symbol $C^*/^*$) and yielded $a=8.620$ (6) Å, $b=13.025(6)$, $c=7.190(5)$, $\beta=116°15'$. These cell data fall in the range for low sanidine as given by Wright & Stewart (1968).

Glass. Glass appeared above 740°C in unbuffered runs of fluoro-zinnwaldite composition, above 810°C in runs of fluoro-polylithionite composition. In buffered runs, glass appears above ~750°C. The latter glass is colorless and probably quite low in iron. Neither chemical composition nor refractive index were determined. This glass coexists with mica.

Kalsilite. Kalsilite is one of the breakdown products of iron-rich micas on the siderophyllite-polylithionite join and coexists with mica and hercynite-magnetite solid solution. It could be observed as fragments or rare lath-shaped cross sections (both length-fast and length-slow). Refinement of powder data (four diffractions) gave $a=5.161(7)$ Å and $c=8.73(4)$, which overlap with values given by Smith and Tuttle (1957).

Hercynite-magnetite. Because the charge in buffered runs is invariably contaminated with graphite, members of hercynite-magnetite series could be identified from X-ray patterns only. Composition of solid solutions was determined from cell edge according to Turnock and Eugster (1962). Cell data for hercynites and magnetites appear in Table 4 and Figure 5.

Lithium metasilicate. Li_2SiO_3 ought to accompany sanidine formed by breakdown of polylithionite: $K_2Li_4Al_2Si_8O_{20}F_4+2H_2O\rightarrow 2KAlSi_3O_8+2Li_2SiO_3+4HF$. Diffractions of lithium metasilicate (Austin, 1947 and calculated from data of Donnay & Donnay, 1953), however, were not

TABLE 3. SELECTED EXPERIMENTS ON SIDEROPHYLLITE-POLYLITHIONITE MICAS IN EQUILIBRIUM WITH CFG/NNO BUFFER AT 2 kbar AND CELL DATA FOR RESULTING MICAS

Run No.[a]	Reactants[b,c]	T, °C (measured)	Time, hours	Products[b]	a, Å	b, Å	d (001), Å	β, °
0–6	F-polylithionite mix	(612½–621)	(110)[d]	mi	5.189 (2)	8.962 (4)	9.881 (5)	100.20 (5)
0–8	F-mi	561¼–567½	625¼	mi	5.193 (3)	8.969 (4)	9.897 (7)	100.13 (6)
0–9	F-mi	596 –627	625¼	mi+san	5.192 (3)	8.966 (6)	9.890 (7)	100.18 (6)
0–10	F-mi	707½–713¾	601	san[e]+lim(?)+mi	—	—	—	—
0–11	F-mi	723½–734¼	589½	san+mi+lim+l	—	—	—	—
0–15	F-mi	754 –758	649	san+mi	—	—	—	—
0–18	F-mi	784 –788	621	san+l	—	—	—	—
0–19	F-plgl[f]	739 –743	661	san+l[g]	—	—	—	—
3–3	$F_2(OH)_2$-mi	558½–569¾	595	mi	5.264 (5)	9.116 (4)	10.003 (4)	100.50 (10)
3–4	$F_2(OH)_2$-mi	642½–647¾	667	mi+san	5.269 (3)	9.128 (3)	10.027 (5)	100.31 (6)
3–5	$F_2(OH)_2$-mi	463 –470½	1287	mi	5.262 (4)	9.112 (5)	9.997 (6)	100.47 (9)
3–7	$F_2(OH)_2$-mi+F-plgl[f]	558¾–562	664	mi+san	5.205 (5)	9.017 (5)	9.930 (9)	100.14 (10)
3–10	$F_2(OH)_2$-mi	807 –812½	661	mi+l	5.312 (2)	9.202 (3)	10.056 (2)	99.90 (3)
4–5	$F_2(OH)_2$-mi	562½–573¼	673¼	mi	5.284 (3)	9.152 (3)	10.048 (4)	100.33 (6)
4–6	$F_2(OH)_2$-mi	705 –716¾	589½	mi+san+lim(?)	5.293 (2)	9.168 (3)	10.054 (4)	100.17 (4)
4–7	$F_2(OH)_2$-mi+F-plgl[f]	643 –647½	598	mi+san	5.261 (3)	9.106 (5)	10.018 (8)	100.09 (10)
5–5	$F_2(OH)_2$-mi	558¼–565	593¼	mi	5.303 (4)	9.180 (4)	10.071 (4)	100.24 (7)
5–6	$F_2(OH)_2$-mi	702¾–715	667	mi	5.299 (2)	9.179 (3)	10.062 (4)	100.08 (5)
5–7	$F_2(OH)_2$-mi	754 –763	624	mi+l	5.308 (3)	9.194 (4)	10.067 (4)	100.05 (5)
5–11	$F_2(OH)_2$-mi+F-plgl[f]	709½–715	715	mi+san	5.263 (3)	9.106 (4)	10.005 (5)	100.21 (6)

6–5	$F_2(OH)_2$-mi	$538\frac{3}{8}$–$547\frac{1}{2}$	602	mi	5.319 (3)	9.203 (4)	10.089 (4)	100.16 (6)
6–6	$F_2(OH)_2$-mi	$755\frac{1}{2}$–774	602	mi+ks+mt(?)	5.326 (3)	9.225 (4)	10.078 (3)	100.16 (5)
6–7	$F_2(OH)_2$-mi+F-plgl[f]	$750\frac{1}{2}$–755	598	mi+l+lc(?)	5.292 (3)	9.176 (5)	10.050 (5)	100.05 (5)
6–9	$F_2(OH)_2$-mi	808 –812	933	mi+ks+mt	5.330 (3)	9.238 (4)	10.065 (4)	100.03 (6)
7–9	$F_2(OH)_2$-mi	$550\frac{1}{4}$–$552\frac{1}{2}$	608	mi	5.336 (3)	9.236 (4)	10.092 (4)	100.35 (5)
7–10	$F_2(OH)_2$-mi	757 –$769\frac{1}{4}$	588	mi+hc+ks	5.330 (2)	9.244 (3)	10.076 (3)	100.04 (4)
7–11	$F_2(OH)_2$-mi	$705\frac{1}{2}$–709	$652\frac{1}{2}$	mi+hc+ks	5.333 (3)	9.244 (4)	10.082 (5)	100.06 (6)
7–13	$F_2(OH)_2$-mi	$800\frac{1}{2}$–804	564	mi+hc+mt+ks	5.336 (3)	9.245 (4)	10.064 (4)	100.01 (7)
7–14	$F_2(OH)_2$-mi	638–$643\frac{1}{2}$	564	mi+hc+ks	5.334 (3)	9.249 (4)	10.088 (4)	100.05 (5)
8–9	$F_2(OH)_2$-mi	$556\frac{3}{4}$–560	588	mi	5.357 (4)	9.276 (4)	10.101 (4)	100.30 (6)
8–10	$F_2(OH)_2$-mi	$712\frac{3}{4}$–$714\frac{3}{4}$	285					
		$733\frac{1}{2}$–$747\frac{1}{2}$	$292\frac{1}{2}$	mi+hc+ks[e]	5.363 (3)	9.283 (3)	10.089 (5)	100.10 (6)
8–11	$F_2(OH)_2$-mi	$699\frac{1}{4}$–$704\frac{1}{4}$	$652\frac{1}{2}$	mi+hc+ks	5.363 (2)	9.285 (3)	10.102 (3)	100.03 (4)
8–13	$F_2(OH)_2$-mi	656 –$660\frac{1}{2}$	664	mi+hc+ks	5.358 (2)	9.282 (2)	10.097 (3)	100.07 (4)
8–15	$F_2(OH)_2$-mi	598 –604	620	mi+hc+ks	5.360 (3)	9.280 (3)	10.102 (3)	100.17 (5)
8–16	$F_2(OH)_2$-mi	804 –809	933	mi+hc+ks+san(?)	5.360 (4)	9.278 (5)	10.088 (6)	99.97 (8)

[a] The first digit in the run number is the coefficient x in sid_xpl_{8-x} and represents the composition of the reactant mica.

[b] Vapor is present in all assemblages.

[c] Prefixes F- and $F_2(OH)_2$- refer to composition of the mix from which the mica was grown.

[d] This mica was not buffered. It grew in 110 hours from the mix.

[e] Cell dimensions in text.

[f] The glass contains some crystals of LiF.

[g] Plus a small quantity of unidentified crystalline phase(s).

hc=hercynite; ks=kalsilite; l=liquid; lc=leucite; lim=lithium metasilicate; mi=mica; mt=magnetite; plgl=polylithionite glass; san=sanidine.

TABLE 4. CELL EDGE FOR MEMBERS OF HERCYNITE-MAGNETITE SERIES COEXISTING WITH MICAS ON THE SIDEROPHYLLITE-POLYLITHIONITE JOIN AT 2 kbar. ATMOSPHERE CONTROLLED BY CFG/NNO BUFFER

Run No.[a]	a, Å	Run No.	a, Å
6–9	8.361 (7)	7–14	8.199 (3)
7–10	8.230 (8)	8–10	8.214 (4)
7–11	8.214 (6)	8–11	8.198 (3)
7–13	8.250 (16)	8–13	8.186 (2)
	&	8–15	8.175 (6)
	8.351 (6)	8–16	8.226 (3)

[a] The first digit in the run number is the coefficient x in sid_xpl_{8-x} and represents the composition of the starting mica. See also Table 3.

observed on X-ray patterns of the breakdown assemblage even if it was depleted in sanidine by hand-picking. A phase similar to lithium metasilicate could be observed optically in products of runs at ~750°C. Munoz (1966) also observed an inconsistent behavior of this phase and postulated that it is a stable phase at low f(HF). In the present experiments, I assume lithium metasilicate to be a stable phase.

α-eucryptite. In unbuffered runs with OH-zinnwaldite (T = ~750°C) α-eucryptite crystals coexisted with leucite and magnetite. Measurements on a two-circle goniometer identified forms $m\{10\bar{1}0\}$, $a\{11\bar{2}0\}$, $r\{10\bar{1}1\}$, $S\{01\bar{1}2\}$, $j\{12\bar{3}5\}$, $p\{4\bar{1}32\}$ (?), and $c\{0001\}$. The c:a(morph) = 0.6705 is close to single-crystal X-ray c:a = 0.6683. Precession photographs show extinctions of R*, morphology corresponds to point group $\bar{3}$ (Laue class $\bar{3}$); these identify the space group as $R\bar{3}$. The cell dimensions are a = 13.520(4) Å, c = 9.035(4) (a(rh) = 8.367, α = 107°48′), refractive indices ω = 1.577(1), ϵ = 1.589(1), D(meas) = 2.67 gmc^{-3} is bigger than D(calc) = 2.63, perhaps due to magnetite inclusions. After deducting from the bulk composition of the charge $KAlSi_2O_6$ for leucite and $Fe^{2+}Fe_{1.85}^{3+}Al_{0.15}O_4$ for a magnetite solid solution, the composition of eucryptite should be close to $Li_{6.12}Al_{5.80}Si_{6.12}O_{24}$ (Z = 3.045). α-eucryptite is not a stable phase in assemblages equilibrated with the CFG/NNO buffer at 2 kbar.

Lithium fluoride. In a few unbuffered runs at 2 kbar and 810°C, lithium fluoride was associated with glass. It was identified by X-ray powder pattern. Lithium fluoride is not a stable phase in assemblages equilibrated with CFG/NNO buffer at 2 kbar.

Experiments on Annite

Experiments were performed at 2 kbar to test the effect of fluorine control on annite. Annite was synthesized from OH and $F_2(OH)_2$ mixes and exposed to an HF-controlled atmosphere for different periods of time at about 560°C. The response of annite to buffering was assessed from $d(001)$, which is considerably different for both starting materials.

The $d(001)$ of $F_2(OH)_2$-annite[1], which is lower than that of OH-annite, increases in about 60 hours of buffering to a value close to $d(001)$ of OH-annite and does not change further with time. The same holds for $d(001)$ of $F_2(OH)_2$-annite pre-equilibrated with the NNO buffer. These experiments demonstrate that the buffer can deplete the charge in fluorine at a high rate. Experiments designed to show that the buffer can supply fluorine failed because $d(001)$ of fluorine-free annite overlaps with that of $F_2(OH)_2$-annite buffered with respect to fluorine (Fig. 2). It is, however, likely that an equilibrium composition was approached in these experiments and that it is close to OH-annite, as indicated also by optical similarity between OH and buffered annite. It is interesting that phlogopite extracts fluorine from the gas phase (Munoz and Eugster, 1969). Data on annite indicate that it differs from phlogopite in this respect.

The reaction of buffered (OH,F)-annite to sanidine+magnetite +vapor was reversed at ~570°C and 2 kbar (Table 2). In absence of fluorine and with NNO buffer, the analogous reaction of OH-annite takes place at ~630° and 2070 bars (Eugster and Wones, 1962). The value of $f(H_2)$ for the former reaction at $T=570$°C can be interpolated in Munoz and Eugster's (1969) table as 4.460 bar. From the regression relation of $\log K$(OH-annite) on $1/T$, $f°(H_2)$ at $T=570$°C can be calculated as 0.966 $\pm$.240 bar (Wones and Eugster, 1965). The activity of OH-annite in the (OH,F)-annite at 570°C is then $a=f(H_2)/f°(H_2)=4.92$ (± 1.22). The fact that the activity is larger than unity is probably due to the metastability of standard state; OH-annite is not stable at the given f(HF) and p. This activity may reflect also the unknown proportion of oxy-annite in the synthetic annite to which refer the data of Wones and Eugster (1965).[2]

[1] The compositions are given in terms of starting mix.

[2] Dr. D. R. Wones of M.I.T. (priv. comm.) suggested two alternate explanations: (i) In view of the long run times (Table 2), nickel in the NNO buffer may alloy with silver from the capsules and change the buffer assemblage to (Ni, Ag)-NiO. (ii) There may be disequilibrium between the hydrogen buffer and the charge. According to either alternative, the $f(H_2)$ in the charge would be lower than calculated for the NNO buffer, lowering thus the apparent reaction temperature. Should the activity be less than or equal to one, a temper-

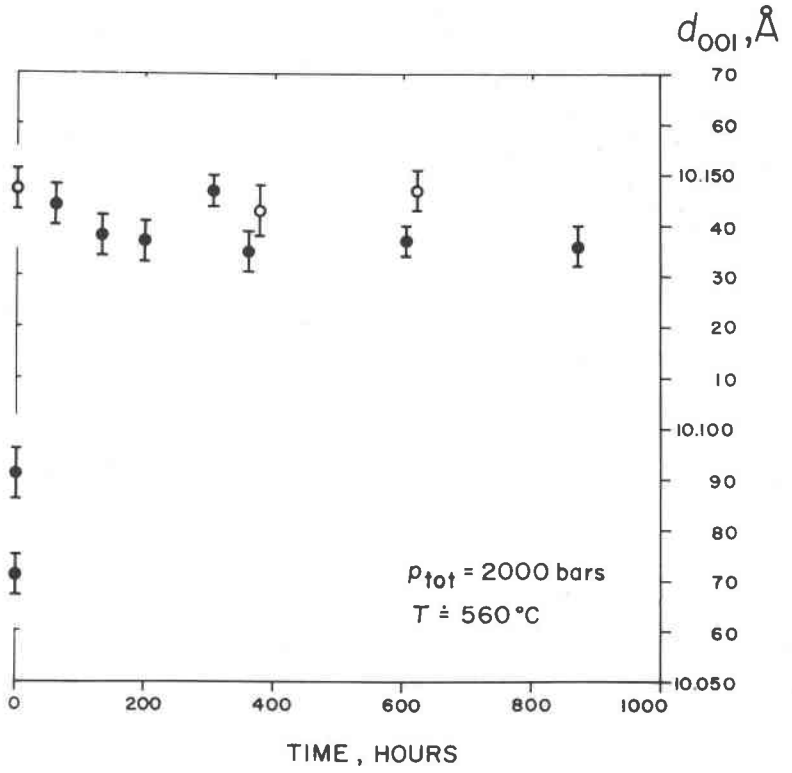

FIG. 2. $d(001)$ of synthetic annite allowed to equilibrate with the CFG/NNO buffer for different periods of time. Solid circles = experiments with $F_2(OH)_2$-annite as starting material; open circles = experiments with OH-annite as starting material.

Synthetic annite has not been analyzed. A linear interpolation between $d(001)$ of OH-annite and of F-annite (Shell and Ivey, 1969) shows that the $F_2(OH)_2$ mix yields annite with F/(F+OH) between 0.34 and 0.46.[1]

EXPERIMENTS ON SIDEROPHYLLITE-POLYLITHIONITE MICAS

The siderophyllite-polylithionite micas required at least 600 hours to equilibrate with the fluorine buffer. They were not analyzed, and thus

ature shift of at least 60°C has to be invoked. I have not examined the metal in the NNO buffer after experiments and have no indication of equilibrium between the hydrogen buffer and the charge other than a fairly convincing reversal of the reaction. The problem remains open and more work on it is needed.

[1] Shell and Ivey's F-annite was grown at 1 bar and 800°C and has parameters $a = 5.310$ Å, $b = 9.260$, $d(001) = 9.982$, $\beta = 100.12°$ ($\beta' = 95.00°$).

there is no direct evidence on their contents of F, OH, O, or H_3O. It appears safe not to consider calcium as a component in compositions of mica and most of its reaction products; this may be wrong in melting reactions, as calcium may be appreciably soluble in the melt.

Siderophyllite. In experiments on siderophyllite composition, siderophyllite (including its cation-deficient variety), kalsilite, hercynite, and vapor are the phases observed. These can be expressed by seven components, $KAlSiO_4$,SiO_2,Al_2O_3,Fe,H_2,O_2,F_2 (Fig. 3). At high temperatures, hercynite has the composition $Fe^{2+}(Fe_{0.5}^{3+}Al_{1.5})O_4$, which can be used as a component; the system can be treated in terms of six components.

Up to ~560°, fluorine-containing siderophyllite[1] is the only solid phase stable i.e.w. the CFG/NNO buffer (Fig. 4). Above 560°C, siderophyllite is accompanied by hercynite and kalsilite, whose proportion relative to siderophyllite increases with temperature (Fig. 5f). Having no analytical data on the siderophyllite coexisting with kalsilite and hercynite, I propose the following model for this reaction:

$$8K_2Fe_4^{2+}Al_2Al_4Si_4O_{20}(OH, F)_4 + (0.0, 4.61)O_2$$
$$\rightarrow 4.73K_{1.69}Fe_{3.38}^{2+}Al_{2.16}Al_{2.92}Si_{5.08}O_{20}(OH, F)_4 + 8KAlSiO_4$$
$$+ 10.67Fe^{2+}(Fe_{0.5}^{3+}Al_{1.5})O_4 + 6.55(H_2, F_2) + (1.94, 0.0)O_2.$$[2]

This equation is tentative for several reasons: (i) It would have to be rewritten for different temperatures to account for the temperature-dependent proportions of hercynite, kalsilite, and mica. (ii) Composition of the spinel is $hc_{75}mt_{25}$ only at about 790°C (Fig. 5e), which is not true at other temperatures; then the compositions of reacting phases define a solid or a tilted plane in the tetrahedron of Figure 3. (iii) Total trivalent iron in the charge should increase with $f(O_2)$ imposed by the NNO buffer, and thus some iron in siderophyllite may be trivalent. (iv) Interlayer vacancies may be filled with hydronium, and the charge balanced (as in case of Fe^{3+}) by more octahedral vacancies or by oxygen replacing (OH,F).

The equation shows the feasibility of appearance of kalsilite and spinel compensated by absorption of silica by the mica. Even though there may be some silica in the vapor phase, the cation-deficient siderophyllite is likely the most efficient silica-extractor. This is indirectly supported by the fact that no additional silicate phases were observed in the charge or

[1] All reactions take place in the presence of gas.

[2] Hydrogen and oxygen would react to water; the equation was written so as to apply to both hydroxy- and fluoro-siderophyllite.

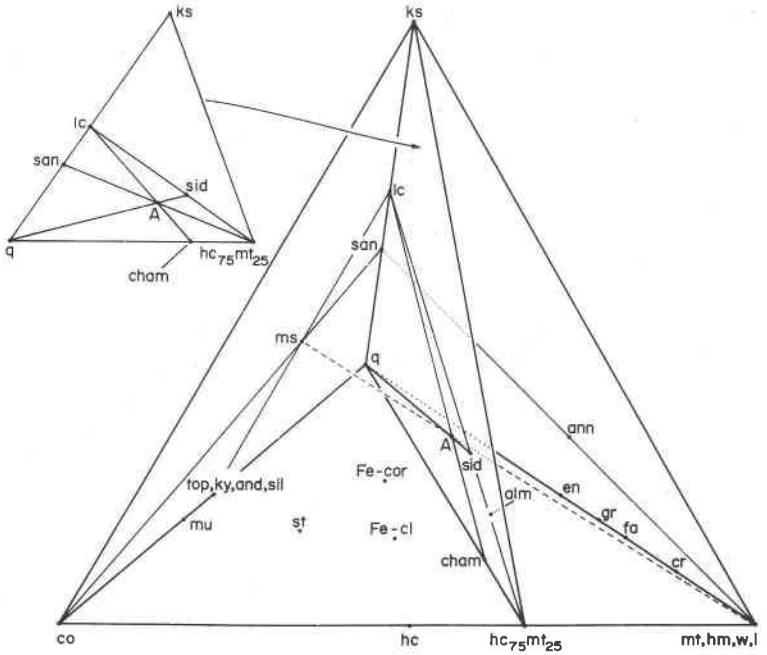

FIG. 3. Compositions of phases in the system, $KAlSiO_4$-SiO_2-Al_2O_3-Fe-(F-H-O) vapor. Point A represents composition $K_{1.69}Fe_{3.38}^{2+}Al_{2.16}Al_{2.92}Si_{5.08}O_{20}(OH,F)_4$. alm = almandine; and = andalusite; ann = annite; cham = chamosite; co = corundum; cr = cronstedtite; en = enstatite; fa = fayalite; Fe-cl = iron-chloritoid; Fe-cor = iron-cordierite; gr = greenalite; hc = hercynite; hm = hematite; i = iron: ks = kalsilite; ky = kyanite; lc = leucite; ms = muscovite; mt = magnetite; mu = mullite; q = quartz; san = sanidine; sid = siderophyllite; sil = sillimanite; st = staurolite; top = topaz; w = wüstite.

the fluorine buffer of sid_8pl_0 and sid_7pl_1 runs (except for 8–16; see below) and that most natural lithium-iron micas, the iron-rich ones in particular, are cation-deficient (Rieder, *et al.*, 1970). According to Figure 3, composition A (the product mica in the above equation) can react to sanidine $+hc_{75}mt_{25}$[1]. If richer in silica than A, the mica can react with kalsilite to sanidine$+hc_{75}mt_{25}$. In the X-ray pattern of products of run 8–16 (804–809°C), three weak diffractions correspond to three strongest sanidine lines. Combined with the decline of kalsilite and increase of spinel in 8–16 (Fig. 5f), it indicates that this mica, indeed, reached an advanced stage of cation deficiency and reacted with kalsilite to sanidine and spinel. The above evidence, although indirect, supports thus correctness of the model reaction.

It is interesting that the mica's tendency to create vacancies and thus

[1] Composition A can react also to muscovite+iron oxide.

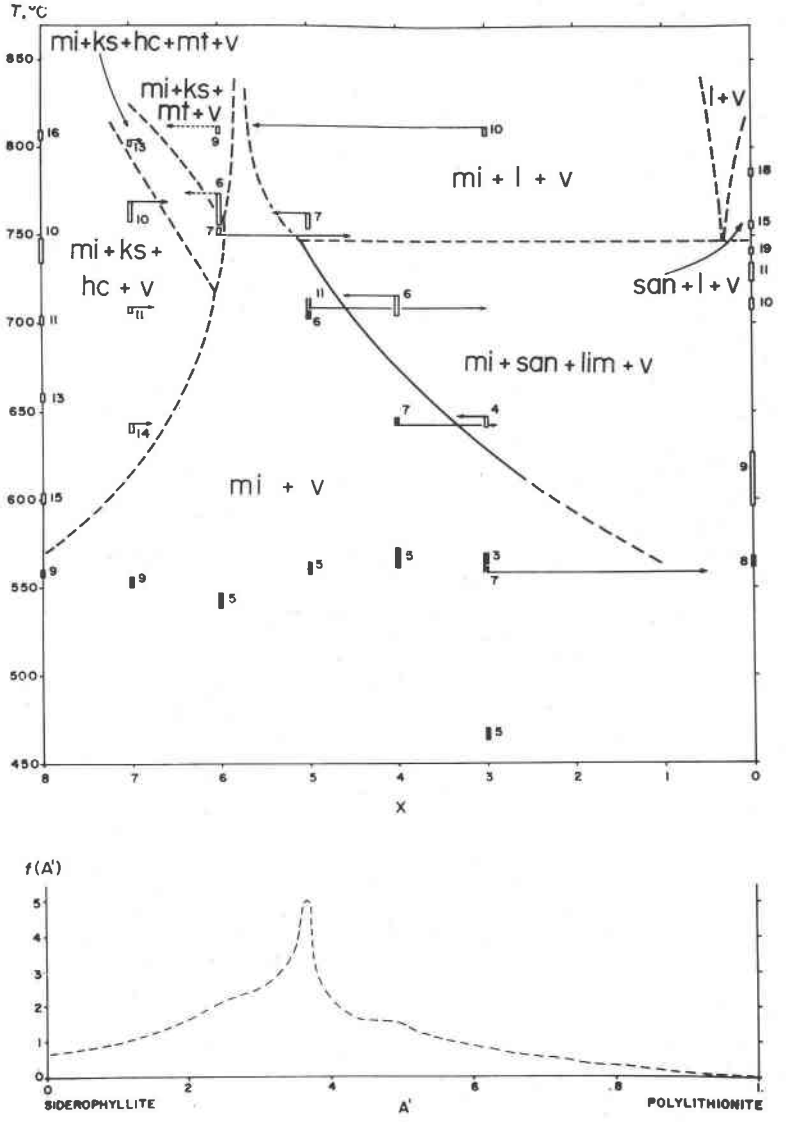

FIG. 4. T-X plot for the siderophyllite-polylithionite join at 2 kbar. The assemblages are in equilibrium with calcite-fluorite-graphite, $f(H_2)$ of the NNO buffer is imposed externally. x is the coefficient in $sid_x pl_{8-x}$ and represents the first digit in the run number; the second digit is written next to every experimental point. Inferred boundaries and boundaries not based on reversals are dashed. Assuming that a set of analyses of natural micas (Rieder *et al.*, 1970) is a random sample, the estimated probability density function for their composition, $f(A')$, is plotted against the ratio A′ (bottom of figure). hc=hercynite; ks=kalsilite; l=liquid; lim=lithium metasilicate; mi=mica; mt=magnetite; san=sanidine.

to absorb silica is so strong that the mica coexists with the silica-undersaturated kalsilite. Silica activity in both phases being identical, such a mica is equally incompatible with quartz as kalsilite itself. Most natural assemblages of lithium-iron micas contain quartz; it is not surprising that these micas are considerably cation-deficient (Rieder, *et al.*, 1970)[1]. The equation on p. 269 links cation-deficiency of siderophyllite to fugacities of volatiles: In absence of fluorine, high $f(H_2)$ and $f(O_2)$ prevent growth of cation-deficient micas. Inversely, in the presence of fluorine, high $f(O_2)$ is essential for their growth. Along with other factors that complicate the reaction, this may well account for the irregularity of the number of vacancies in natural micas. It has not been possible to compare vacancies in micas from assemblages with and without quartz (too few without quartz), and it is too early to compare them in natural and synthetic micas.

Vacancies in siderophyllite conceivably affect the cell dimensions. From a good agreement between a and b for cation-deficient natural and stoichiometric synthetic micas (see next chapter) one can expect small, if any, changes of siderophyllite's a and b. This is what is observed (Fig. 5a,b). $d(001)$ could change considerably with vacancies if ordering of the structure took place at the same time. The decrease of $d(001)$ with vacancies is, however, decidedly smaller than expected (Fig. 5c). The $f(HF)$ used is perhaps too low to promote ordering of the octahedral cations (see below). The lack of sensitivity of cell dimensions to vacancies has two consequences: (i) From inspection of cell parameters of a mica one will likely fail to recognize its cation-deficiency. (ii) If cell dimensions of deficient lithian siderophyllite behave like those of siderophyllite, the position of such a mica on the siderophyllite-polylithionite join can be estimated from its cell data without much bias.

Polylithionite. Polylithionite, sanidine, lithium metasilicate, liquid, and vapor were observed in experiments on polylithionite composition. These can be described by four components, $KAlSi_3O_8$, Li_2SiO_3, H_2O, and HF. Theoretically, compositions of mica and liquid span across the tetrahedron of Figure 6a, and the compositions of phases can be projected onto the triangle, sanidine - lithium metasilicate - vapor (Fig. 6b). The system

[1] Following the procedure used in that paper, the ratio of octahedrally created octahedral vacancies to those created tetrahedrally in mica A is calculated as 2.0, which is identical with the values obtained for natural lithium-iron micas. The hypothetical fully occupied formula calculated from the cation-deficient formula A differs, however, from the formula of fully occupied siderophyllite. This may be due to simplifying assumptions on which the calculation of vacancies rests or it may indicate that the vacancy-forming process in natural micas differs from that in the experimental system chosen.

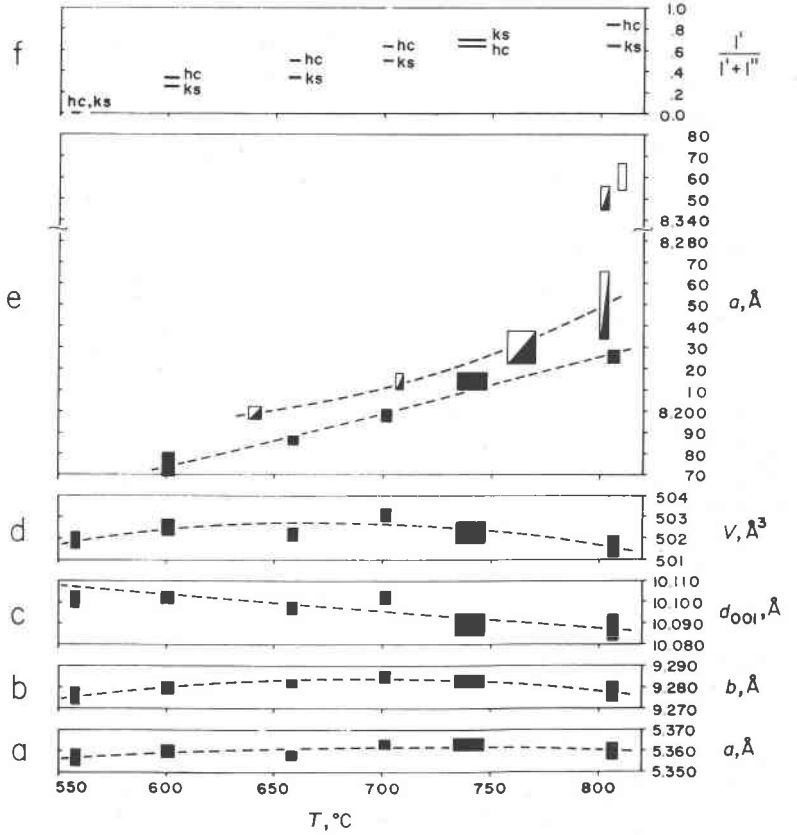

FIG. 5. Change of cell dimensions of siderophyllite (a through d) and of members of the hercynite-magnetite series (e) with temperature. Total pressure is 2 kbar, phases are in equilibrium with the CFG/NNO buffer. Solid rectangles = bulk composition sid_3pl_0; black-and-white rectangles = bulk composition sid_7pl_1; open rectangles = bulk composition sid_6pl_2. Sides of rectangles represent uncertainties in the respective parameters. In runs with sid_8pl_0 composition, the proportion of hercynite and kalsilite increases relative to mica with temperature (f): I'' = peak height of $11\bar{3}$ of mica; I' = peak height of 11.0 of kalsilite (ks) or of 220 of hercynite (hc).

degenerates to a three-component one, whose invariant point can be analyzed. If polylithionite reactions are treated in a four-component system, the invariant assemblages must contain six phases each. Five have been observed at constant pressure; there may be a sixth phase in the system, stable perhaps at another p. This phase might be another liquid as postulated by Munoz (1966) and supported by Kogarko's (1967) observation that the presence of fluorine in experimental systems increases chances of liquid immiscibility.

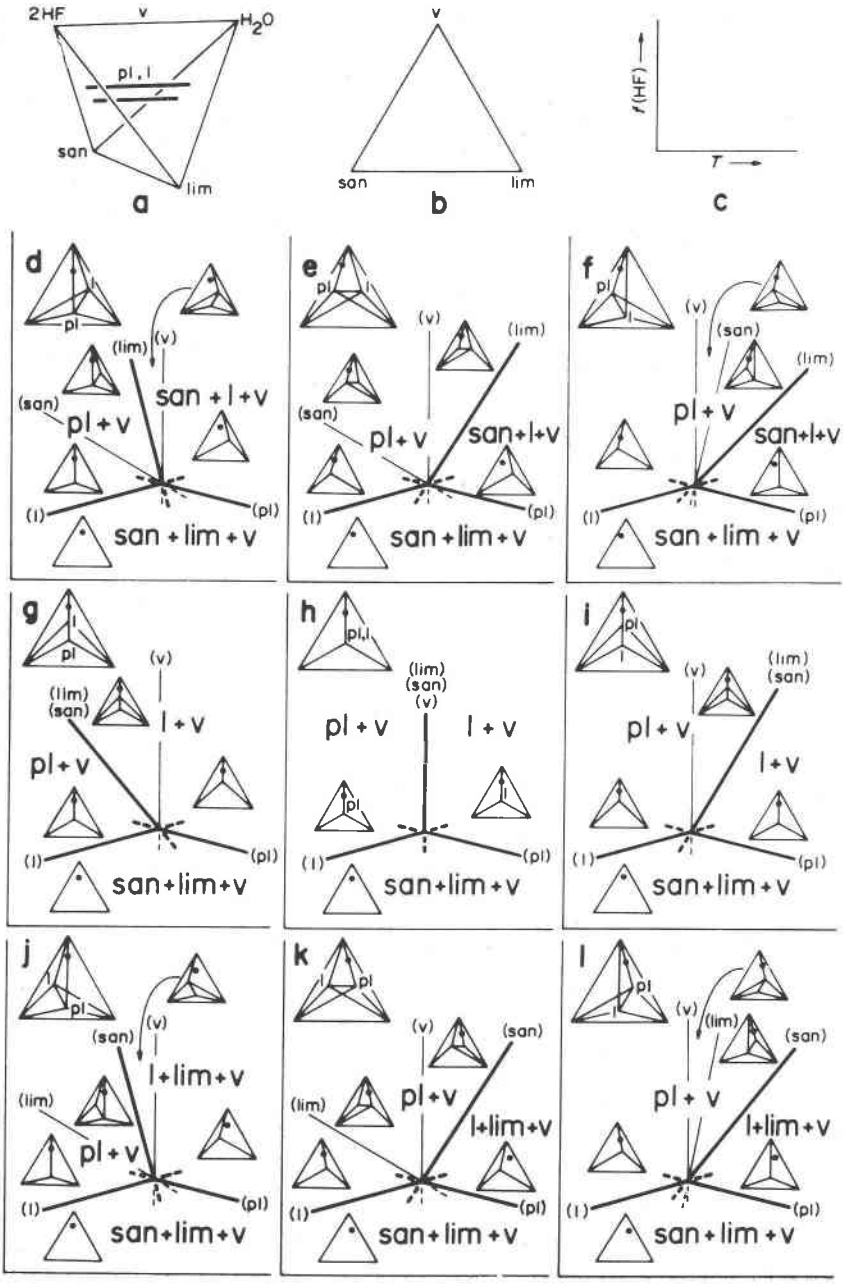
2HF
v
H2O
pl, l
san
lim
a
v
san
lim
b
f(HF)
T
c
d
pl
l
(lim)
(v)
(san)
san + l + v
pl + v
(l)
(pl)
san + lim + v
e
pl
l
(v)
(lim)
(san)
pl + v
san+l+v
(l)
(pl)
san + lim + v
f
pl
l
(v)
(san)
(lim)
pl + v
san+l+v
(l)
(pl)
san + lim + v
g
l
pl
(v)
(lim)
(san)
l + v
pl + v
(l)
(pl)
san+lim+v
h
pl,l
(lim)
(san)
(v)
pl + v
l + v
pl
l
(l)
(pl)
san+lim+v
i
pl
l
(v)
(lim)
(san)
pl + v
l + v
(l)
(pl)
san+lim+v
j
pl
l
(san)
(v)
l+lim+v
(lim)
pl + v
(l)
(pl)
san+lim+v
k
l
pl
(v)
(san)
(lim)
pl + v
l+lim+v
(l)
(pl)
san + lim + v
l
pl
l
(v)
(lim)
(san)
pl + v
l+lim+v
(l)
(pl)
san + lim + v

Above ~550°C, polylithionite reacts to sanidine+lithium metasilicate. Melt plus sanidine are stable above ~750°C. There is *no proof* that polylithionite is stable below 550°C, i.e.w. CFG/NNO buffer at 2 kbar: Its reaction to sanidine+lithium metasilicate is very sluggish and was not reversed. Sanidine is not stable in fluoro-polylithionite system at 2 kbar (Munoz, 1966) and thus cannot persist metastably from fluorine-rich starting compositions; it is a stable phase under the presently used conditions.

Problems of polylithionite reactions are better understood, but not solved, by analyzing them in an $f(\mathrm{HF})-T$ plane (Fig. 6c through l). With increasing temperature at low $f(\mathrm{HF})$, pl+v should react to san +lim+v and later to san+l+v if the chemography is any of d,e,f in Figure 6. This chemography cannot, however, explain the reaction pl +v→l+v reported by Munoz (1966) at apparently high $f(\mathrm{HF})$; such a case is compatible with any of g,h,i in Figure 6. Both observations are explicable if the chemical compositions of polylithionite and liquid change from d,e,f, to g,h,i as $f(\mathrm{HF})$ increases. Experiments on bulk compositions other than pl+v are needed to single out the chemographies involved.

Cell dimensions of polylithionite that persists metastably at high temperatures are very close to those of the octahedrally ordered starting fluoro-polylithionite (cf. runs 0–9 and 0–8 with 0–6 in Table 3). The slight increase of $d(001)$ may indicate entrance of some (OH) into the structure preceding the mica's decomposition. This difference in layer thickness is much too small to rank such a mica with other synthetic octahedrally disordered micas (more discussion below). Hence this mica is likely not equilibrated with the buffer and thus metastable. The same may be true of polylithionite "stable" in 100 percent yields at low temperatures, but exceedingly long run times may be needed to prove this.

Solid solution siderophyllite-polylithionite. Compositions and reactions of micas in the middle of the siderophyllite-polylithionite join have to be

FIG. 6. Analysis of phase relations in an isobaric section through the phase diagram of the system, $KAlSi_3O_8$ (san)-Li_2SiO_3(lim)-H_2O,2HF(v). The tetrahedron (a) is projected onto the san-lim-v plane (b) and the isobaric invariant points analyzed in an $f(\mathrm{HF})$-T plane (c). Nine cases are distinguished according to the compositional relation between polylithionite (pl) and liquid (l). Phase assemblages for the bulk composition polylithionite +vapor (marked with a solid circle) are labeled and the corresponding divariant fields separated by heavy lines.

treated in an eight-component system, $KAlSiO_4$-SiO_2-Al_2O_3-Fe-Li_2SiO_3-H_2-O_2-F_2.

Under the conditions used, lithium-iron micas have an extensive stability field, particularly below 550°C. Compositions between sid_6pl_2 and sid_5pl_3 are stable to temperatures above 800°C (Fig. 4). Micas rich in lithium react to mica+sanidine+lithium metasilicate and coexist with melt at high temperatures. Iron-rich micas react to a cation-deficient mica+kalsilite±hercynite±magnetite. The cation-deficient mica is stable to above 800°C, and its deficiency changes with temperature.

At all temperatures studied, siderophyllite is the most cation-deficient composition as indicated by the intensity of kalsilite and hercynite diffractions. The deficiency decreases with increasing lithium and is zero at the disappearance of kalsilite and spinel. The curve separating cation-deficient micas (+kalsilite+spinel) from non-deficient ones in Figure 4 does not express the composition of cation-deficient micas, but represents non-deficient micas richest in iron that can exist at a given temperature. This boundary can be positioned by reaction from above, but not from below, unless the reaction goes to completion. Because the micas equilibrated with the fluorine buffer were fine-grained, only broad ranges of refractive indices could be measured; a possible relation between cation-deficiency and optical properties could not be determined.

Position of the reaction curve mica+vapor→mica+sanidine+lithium metasilicate+vapor was determined from above and below: In the first case, mica+vapor were heated to a temperature at which this mica was expected not to be stable. The product was a mica richer in iron plus sanidine, lithium metasilicate, and vapor. To approach the boundary from below, an Fe−mica+polylithionite glass were combined to yield bulk composition richer in lithium than the mica expectedly stable at the given temperature, and allowed to react. Because of difficulties in preparation of sandine+lithium metasilicate, glass of fluoro-polylithionite composition was used as the polylithionite "component." Its content of fluorine, however, caused difficulties: HF from the glass was apparently trapped by the mica before it could have been consumed by the buffer. This mica, like fluoro-polylithionite, is reluctant to lose fluorine within the run time and retains also a high content of lithium; it is metastable. The tendency of these micas to extract fluorine from the gas is analogous to that of phlogopite (Munoz and Eugster, 1969).

The reaction mi+v→mi+l+v was not reversed. No experiments were performed to determine the position of curves corresponding to reactions mi+l+v⇌l+v and san+l+v⇌l+v.

Figure 5e shows that the spinels coexisting with mica are progressively richer in trivalent iron as the bulk composition of the charge gets richer in lithium and as the temperature increases. Spinels close to the solvus

may not be one-phase as indicated in Figure 4 and Table 4; small quantities of the second spinel can escape attention. The course of boundaries separating the two-phase spinel field in Figure 4 may thus be somewhat incorrect. In terms of phase rule, the $T-X$ section of Figure 4 is not quite satisfactory.

Cell Dimensions of Synthetic Lithium-Iron Micas and Their Relation to Those of Natural Micas

Unit-cell dimensions of synthetic micas were calculated from powder data for all buffered and several unbuffered micas (Table 3). Calibration regression curves of cell parameters on composition were calculated using data for buffered micas that gave 100 percent yields. Single-crystal cell dimensions of natural micas (Rieder *et al.*, 1971) were approximated by regression curves (parameters on composition ratio A′) and plotted on the same grid as the data for synthetic micas.

The agreement between both is excellent for a and good for b (Fig. 7). There is a large difference in $d(001)$ (Fig. 8) and, consequently, V (not shown)[1]. The difference in $d(001)$ is almost 0.1 Å. Because of its agreement for both synthetic and natural micas, parameter a was used to determine composition of reacting micas (endpoints of arrows in Figure 4).[2]

Synthetic micas high in fluorine (not buffered) give $d(001)$ close to those of natural micas; synthetic micas buffered with respect to fluorine, which are apparently low in fluorine, have large $d(001)$ due to lack of octahedral ordering (Rieder, 1968a). In order to check the possibility of transforming the ordered form into disordered, a finely ground natural mica was allowed to equilibrate with the CFG/NNO buffer, but showed only an insignificant increase of $d(001)$, the same being true of synthetic fluoro-polylithionite (see above). These observations strongly indicate that fluorine is involved in octahedral order-disorder phenomena and that, once bound in the ordered structure, is very reluctant to be released.

Natural (ordered) micas exhibit an approximately 1:1 relation between lithium and fluorine. The proper fluorine content is apparently essential for ordering of its structure. If it is proportional to $f(\mathrm{HF})$ in the gas phase,

[1] Bear in mind that the ratio A′ of natural micas is not identical with Li/(Li+Fe) for some lithium-rich compositions; the difference is biggest for $K_2Li_3Al_2Fe^{2+}AlSi_7O_{20}(F,OH)_4$, whose $A'=2/3$ and $Li/(Li+Fe)=3/4$. This, however, is definitely not the cause of the discrepancies between data for synthetic and natural micas inasmuch as there are no data on synthetic micas whose Li/(Li+Fe) is close to 3/4.

[2] Estimation of composition from a using the dashed regression curve in Figure 7 is statistically biased as a regression of Li/(Li+Fe) on a (and not of a on Li/(Li+Fe)) should be used. The error introduced is, however, negligibly small.

then at low f(HF), iron-rich micas ought to grow in the ordered form rather than micas richer in lithium. That this may be so is indicated by a decline of d(001) of 100 percent-yield buffered micas as their composition approaches siderophyllite (Fig. 8).

Geological Application

There are two aspects of experiments on micas with controlled fluorine: First, the data prove again that the stability of micas is a function of

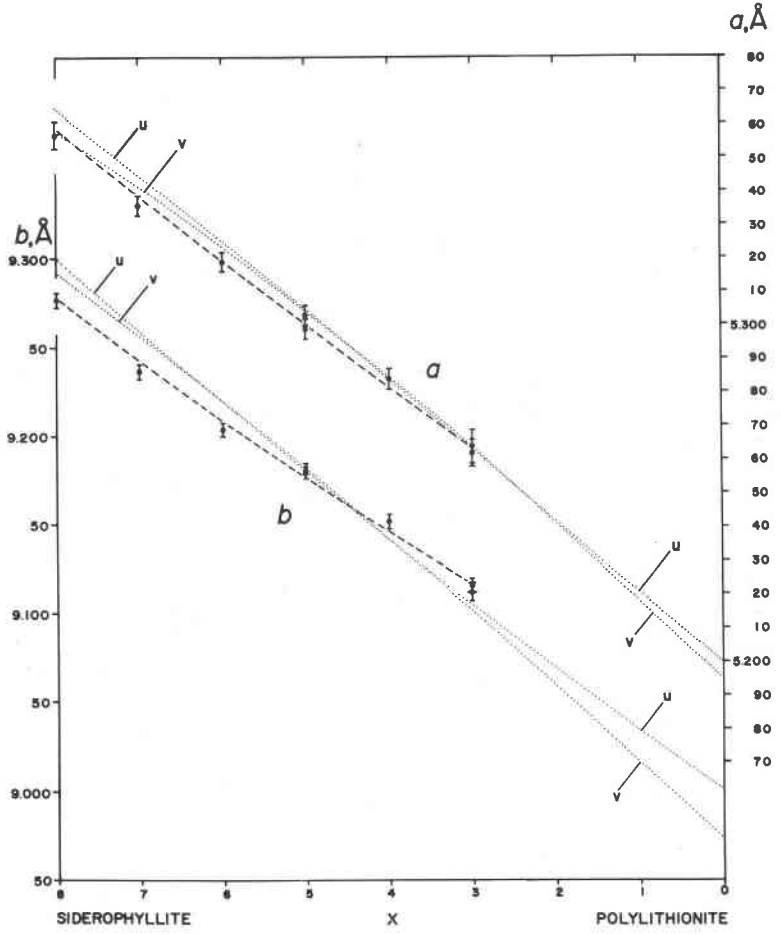

Fig. 7. Cell dimensions a and b of synthetic siderophyllite-polylithionite micas buffered with CFG/NNO at 2 kbar (100% yields only). The broken lines ($a = .000242x^2 + .0164x + 5.212$; $b = .000677x^2 + .0247x + 9.036$; x is the subscript in $sid_x\ pl_{s-x}$) are the regression curves for the data. Regression curves for single-crystal data for natural micas (v just for octahedrally ordered, u for all micas) are dotted.

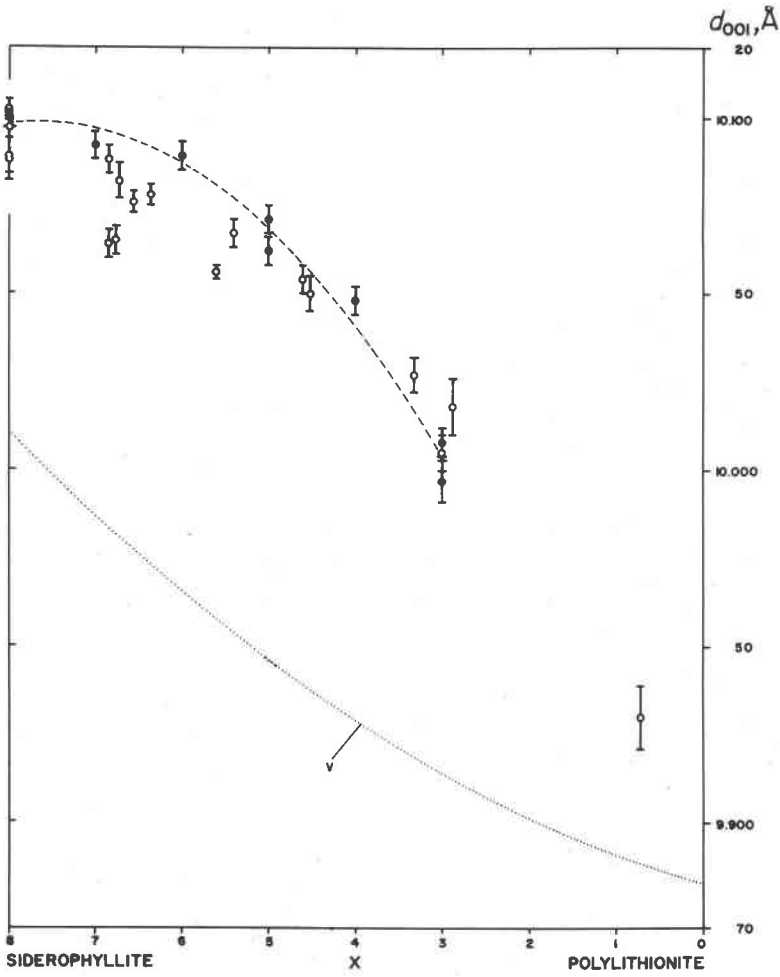

FIG. 8. $d(001)$ of synthetic siderophyllite-polylithionite micas buffered with CFG/NNO at 2 kbar. Solid circles = 100% yields (the corresponding dashed regression curve $d(001) = -.004400x^2 + .0672x + 9.842$; x is the subscript in $sid_x pl_{8-x}$); open circles = data for micas coexisting with other phases. The regression curve v for single-crystal data for octahedrally ordered natural micas (Rieder, 1968a) is dotted.

fluorine content and thus of the $f(HF)$ in gas. Second, data on annite and micas on the siderophyllite-polylithionite join provide insight into the behavior of their natural analogs.

The range of $f(HF)$ in environments of natural lithium-iron micas cannot be estimated quantitatively from the present experiments because natural micas differ substantially from the synthetic ones. Cell

parameters of synthetic siderophyllite-polylithionite micas indicate their octahedral disorder and low fluorine content. Inasmuch as natural micas are high in fluorine and thus octahedrally ordered, it can be merely concluded that f(HF) in experiments was lower than in natural assemblages. It is probable that natural micas grew with an ordered structure. Had they not, their octahedral cations would likely ignore the site-size restrictions of the ordered structure. A solid-state ordering would then produce unmixed phases (with lithium, iron, aluminum), which have not been observed.

It is impossible to calculate f(HF) in greisens as these rocks contain no mineral assemblage that could buffer the rock with respect to fluorine. Štemprok (1965) compiled the important minerals in 285 tin-tungsten-molybdenum deposits (listed is just presence, not coexistence) and found that mica, fluorite, tourmaline, topaz, and apatite are the only widespread fluorine-bearing minerals, of which only fluorite has a stoichiometric content of fluorine. Other minerals needed for buffer assemblages like anorthite, sillimanite, wollastonite, or graphite are unknown from greisens. The presence of minerals with variable fluorine contents means that fluorine in greisens is internally defined, whether imposed by a "pulse" of hydrothermal fluids (Štemprok, 1965) or a "reservoir."

Despite the differences between experiments and reality it is interesting to observe that the most frequent compositions of natural micas coincide with synthetic compositions of highest thermal stability (Fig. 4). This suggests that the geometry of the stability field of the assemblage mica +quartz at high f(HF) is similar to that observed for synthetic low-fluorine micas.

Also, the experimental f(HF) offers a differentiation between the occurrence of annite on one hand and siderophyllite on the other. The decrease of stability of fluorine-buffered annite relative to that of fluorine-free annite explains why annite is not found in fluorine-rich environments. The impossibility of growing fluorine-free siderophyllite when compared to its relatively high stability in an F-controlled atmosphere shows that siderophyllite is the iron mica to occur in media high in fluorine (see also Marakushev and Perchuk, 1970).

Experiments prove that the mica's tendency to contain cation vacancies is strong and related to the silica available and the regime of volatiles. If the mica transforms into a cation-deficient one that coexists with kalsilite, it is logical to expect micas with more vacancies in environments that contain ample silica. It is likely that a wider composition range of deficient micas will be stable in equilibrium with quartz and in micas grown at high f(HF). Zinnwaldite has been reported to replace quartz in greisens (Štemprok, 1960); this relationship is what one would expect

if this mica formed more vacancies in response to an increase of $f(HF)$ and/or T.

Products of experiments done are still remote from the corresponding natural assemblages. Of the phases encountered in experiments (hercynite, kalsilite, lithium metasilicate, magnetite, mica, sanidine) only mica and sanidine are known to occur commonly in greisens (Štemprok, 1965). α-eucryptite, LiF, and leucite, which were grown in unbuffered runs, are unknown or uncommon in greisens. The presence of quartz in natural assemblages demands that it be present in experiments. This should, in my opinion, be preceded by finding a means of detecting cation deficiency of the resulting mica. Experimental work must be expanded to include high $f(HF)$: The assemblage anorthite-fluorite-quartz-topaz, which is close to mineral assemblages of the greisens, is a potential fluorine buffer and probably imposes a more realistic $f(HF)/f(H_2O)$.

Acknowledgments

I am very indebted to Dr. H. P. Eugster for guidance and advice. Discussions held with him were of great help in developing a solid fluorine buffer. He and Dr. G. W. Fisher read the thesis on which this paper is based and made many helpful suggestions. Dr. D. R. Wones critically reviewed the manuscript, and his comments resulted in numerous improvements. The research was aided by NSF Grant GP-5064, H. P. Eugster principal investigator, by the Johns Hopkins University, and by the Ústřední ústav geologický in Praha. All support is gratefully acknowledged.

References

Austin, A. E. (1947) X-ray diffraction data for compounds in systems Li_2O-SiO_2 and BaO-SiO_2. *J. Amer. Ceram. Soc.* **30,** 218–220.

Burnham, C. W. (1962) Lattice constant refinement. *Carnegie Inst. Wash. Year Book* **61,** 132–135.

Donnay, G., and J. D. H. Donnay (1953) Crystal geometry of some alkali silicates. *Amer. Mineral.* **38,** 163–171.

Eugster, H. P., and D. R. Wones (1962) Stability relations of the ferruginous biotite, annite. *J. Petrology* **3,** 82–125.

Kogarko, L. N. (1967) Oblast rassloeniya v rasplavakh sistemy Si, Al, Na||O, F. *Dokl. Akad. Nauk SSSR* **176,** 918–920.

Marakushev, A. A., and L. L. Perchuk (1970) On the influence of the acidity and temperature of postmagmatic solutions on the compositions of micas and chlorite. *In* Z. Pouba and N. Štemprok (eds.) *Problems of Hydrothermal Ore Deposition, Internat. Union Geol. Sci. A. No. 2*: Schweizerbart, Stuttgart, p. 274–278.

Munoz, J. L. (1966) *Synthesis and Stability of Lepidolites.* Ph.D. Thesis, The Johns Hopkins University, Baltimore, Md.

——— (1969) Control of fugacities in fluorine-bearing hydrothermal systems. *Carnegie Inst. Wash. Year Book* **67,** 170–175.

——— and H. P. Eugster (1969) Experimental control of fluorine reactions in hydrothermal systems. *Amer. Mineral.* **54,** 943–959.

Noda, T., and M. Ushio (1964) Hydrothermal synthesis of fluorine-hydroxyl-phlogopite; part two. Relationship between the fluorine content, lattice constants, and the condi-

tions of synthesis of fluorine-hydroxyl-phlogopite. *J. Chem. Soc. Japan, Ind. Chem. Sec.* **67,** 292–297 [Transl.: *Geochem. Intern.* **1,** 96–104 (1964)].

——— AND N. YAMANISHI (1964) Hydrothermal synthesis of fluorine-hydroxyl-phlogopite; part one. The conditions of synthesis of fluorine-hydroxyl-phlogopite and the minerals formed. *J. Chem. Soc. Japan, Ind. Chem. Sec.* **67,** 289—292 [Transl.: *Geochem. Intern.* **1,** 90–95 (1964)].

RIEDER, M. (1968a) Zinnwaldite: Octahedral ordering in lithium-iron micas. *Science* **160,** 1338–1340.

——— (1968b) *A Study of Natural and Synthetic Lithium-iron Micas.* Ph.D. Thesis, The Johns Hopkins University, Baltimore, Md.

——— (1970) Lithium-iron micas from the Krušné hory Mts. (Erzgebirge): Twins, epitactic overgrowths, and polytypes. *Z. Kristallogr.* **132,** 161–184.

———, M. HUKA, D. KUČEROVÁ, L. MINAŘÍK, J. OBERMAJER, AND P. POVONDRA (1970) Chemical composition and physical properties of lithium-iron micas from the Krušné hory Mts. (Erzgebirge). Part A: Chemical composition. *Contrib. Mineral. Petrology* **27,** 131–158.

———, A. PÍCHOVÁ, M. FASSOVÁ, E. FEDIUKOVÁ, AND P. ČERNÝ (1971) Chemical composition and physical properties of lithium-iron micas from the Krušné hory Mts. (Erzgebirge). Part B: Cell parameters and optical data. *Mineral. Mag., (in press.)*

RUTHERFORD, M. J. (1968) *An Experimental Study of Biotite Phase Equilibria.* Ph.D. Thesis, The Johns Hopkins University, Baltimore, Md.

SHELL, H. R., AND K. H. IVEY (1969) Fluorine micas. *Bull. U.S. Bur. Mines* **647,** 1–291.

SMITH, J. V., AND O. F. TUTTLE (1957) The nepheline-kalsilite system: I. X-ray data for the crystalline phases. *Amer. J. Sci.* **255,** 282–305.

ŠTEMPROK, M. (1960) On the genesis of the ore deposit of Cínovec (Zinnwald). *Intern. Geol. Congr., 21st Sess.,* **16,** 43–53.

——— (1965) Genetic features of the deposits of tin, tungsten and molybdenum formation. *In: M. Štemprok* (ed.) *Symposium Problems of Postmagmatic Ore Deposition,* Czechoslovak Academy of Sciences, Praha, **2,** 472–481.

TURNOCK, A. C., AND H. P. EUGSTER (1962) Fe-Al oxides: Phase relationships below 1,000°C. *J. Petrology* **3,** 533–565.

TUTTLE, O. F. (1949) Two pressure vessels for silicate-water studies. *Bull. Geol. Soc. Amer.* **60,** 1727–1729.

VAN VALKENBURG, A., AND R. G. PIKE (1952) Synthesis of mica. *J. Res. [U.S.] Nat. Bur. Stand.* **48,** 360–369.

WONES, D. R. (1963) Physical properties of synthetic biotites on the join phlogopite-annite. *Amer. Mineral.* **48,** 1300–1321.

——— AND H. P. EUGSTER (1965) Stability of biotite: Experiment, theory, and application. *Amer. Mineral.* **50,** 1228–1272.

WRIGHT, T. L., AND D. B. STEWART (1968) X-ray and optical study of alkali feldspar: I. Determination of composition and structural state from refined unit-cell parameters and 2*V*. *Amer. Mineral.* **53,** 38–87.

YODER, H. S., AND H. P. EUGSTER (1954) Phlogopite synthesis and stability range. *Geochim. Cosmochim. Acta* **6,** 157–185.

Manuscript received, July 7, 1970; accepted for publication, October 16, 1970.